

Robust Spin and Charge Excitations Throughout High- T_c -cuprate Phase Diagram From Incipient Mottness

M. Fidrysiak^{1,*} and J. Spałek^{1,†}

¹*Marian Smoluchowski Institute of Physics, Jagiellonian University, ul. Łojasiewicza 11, 30-348 Kraków, Poland*

The generic phase diagram of lightly hole-doped high- T_c -cuprates hosts antiferromagnetic insulating phase with well-defined spin-wave excitations. Contrary to the weak-coupling prediction, these modes persist up to the overdoped metallic regime as intense and dispersive paramagnons. Here we report on our study of the low-energy magnetic and charge excitations within the Hubbard model at strong-coupling, using a modified $1/N$ expansion method with a variational state serving as the saddle point solution. Despite clear separation of magnetic and Hubbard- U energy scales, we find that incipient Mottness affects qualitatively dispersions and widths of magnetic modes throughout entire phase diagram. The obtained magnetic and charge dynamical structure factors agree semi-quantitatively with recent resonant X -ray and neutron scattering data for $\text{La}_{2-x}\text{Sr}_x\text{CuO}_4$ and $(\text{Bi,Pb})_2(\text{Sr,L a})_2\text{CuO}_{6+\delta}$ at all available doping levels. The weak-coupling random-phase-approximation fails already for underdoped samples, pointing to the non-trivial intertwining of distinct energy scales in cuprate superconductors. The existence of a discrete charge mode which splits off the electron-hole continuum is also predicted.

Introduction.—Formulation of fully testable theory of high-temperature superconductivity (HTSC) in the cuprates remains one of the most challenging problems in condensed matter physics. The strongly correlated nature of electrons involved in HTSC, demonstrated in numerous experiments [1–4], provides a firm reference point for theoretical modeling and has been under elaboration for the last two decades [5–8]. The principal features of the phase diagram and other *equilibrium* properties have been reproduced with a degree of success, albeit the pseudogap appearance and associated with it possibility of quantum-critical-point emergence has no unequivocal interpretation as yet [9–11].

A new impetus in the field has been provided by recent developments [12–14] in resonant inelastic X -ray scattering (RIXS), granting access to the detailed structure of spin and charge [15–19] excitations in highly-doped materials. The major experimental finding, consistent among variety of cuprates, is the persistence of intense and dispersive antinodal paramagnons ranging from antiferromagnetic (AF) insulator to overdoped paramagnetic (PM) metal, and their rapid overdamping along the nodal direction [20–30]. Such a selective robustness against damping due to electron-hole (e-h) scattering is inconsistent with weak-coupling prediction and has sparked a discussion about the role those modes may play in HTSC [31–33]. Analogous results have been reported for iron pnictides [34] and iridates [35], pointing towards universality of their presence in correlated materials. Previous theoretical works [36, 37] involved, among others, spin excitations as a viable mechanism of pairing in HTSC. Elucidating the microscopic mechanism underlying this behavior remains a challenge to theory. A successful interpretation of those *dynamic* excitations would also provide a convincing strongly correlated picture of cuprate and related superconductors.

In our approach, the description is divided into the

equilibrium *static* part, driven by a combined effect of local correlations and exchange interactions [10, 38–40], and *dynamic* collective fluctuations around this reference static saddle-point solution. The purpose of this work is to offer the description of the latter dynamic excitations. Namely, in this Letter, we show, starting from the Hubbard-model, that local electronic correlations qualitatively reorganize the magnetic excitation spectrum in hole-doped systems when compared to that resulting from the weak-coupling spin-fluctuation theory. Using a single set of doping independent model parameters for given cuprate family, we reproduce semi-quantitatively experimental magnetic-mode energies and anisotropic paramagnon damping for $\text{La}_{2-x}\text{Sr}_x\text{CuO}_4$ and $(\text{Bi,Pb})_2(\text{Sr,L a})_2\text{CuO}_{6+\delta}$ throughout the phase diagram. To capture the interplay between collective-mode fluctuations and correlated itinerant electrons, a dedicated computational technique extending the variational wave function approach is developed. As a reference point, we discuss the weak-coupling random phase approximation (RPA) results and demonstrate its inadequacy to doped high- T_c cuprates.

Model and method.—We employ Hubbard Hamiltonian $\hat{\mathcal{H}} = \sum_{\sigma,i \neq j} t_{ij} \hat{c}_{i\sigma}^\dagger \hat{c}_{j\sigma} + U \sum_i \hat{n}_{i\uparrow} \hat{n}_{i\downarrow}$, retaining nearest- and next-nearest hopping integrals $t < 0$ and $t' = 0.25|t|$, respectively. Here $\hat{n}_{i\sigma} \equiv \hat{c}_{i\sigma}^\dagger \hat{c}_{i\sigma}$ and U is on-site repulsion. Spin- and charge dynamical susceptibilities are computed using modified $1/N$ expansion (N counts fermionic flavors), so that the saddle point ($N = \infty$) coincides with the variational statistically-consistent (SGA) solution [10, 11, 40]. This allows to capture both the Mott physics and long-wavelength collective excitations already at the leading expansion order. The present technique is formulated in terms of Grassmann variables ($\bar{\eta}_i^\alpha$ and η_i^α), describing itinerant electrons, Grassmann bilinears $\hat{P}_i^{(\alpha,\beta,\delta i,\text{Re})} \propto [\bar{\eta}_{i+\delta i}^\alpha \eta_i^\beta + \bar{\eta}_i^\beta \eta_{i+\delta i}^\alpha]/2$, $\hat{P}_i^{(\alpha,\beta,\delta i,\text{Im})} \propto$

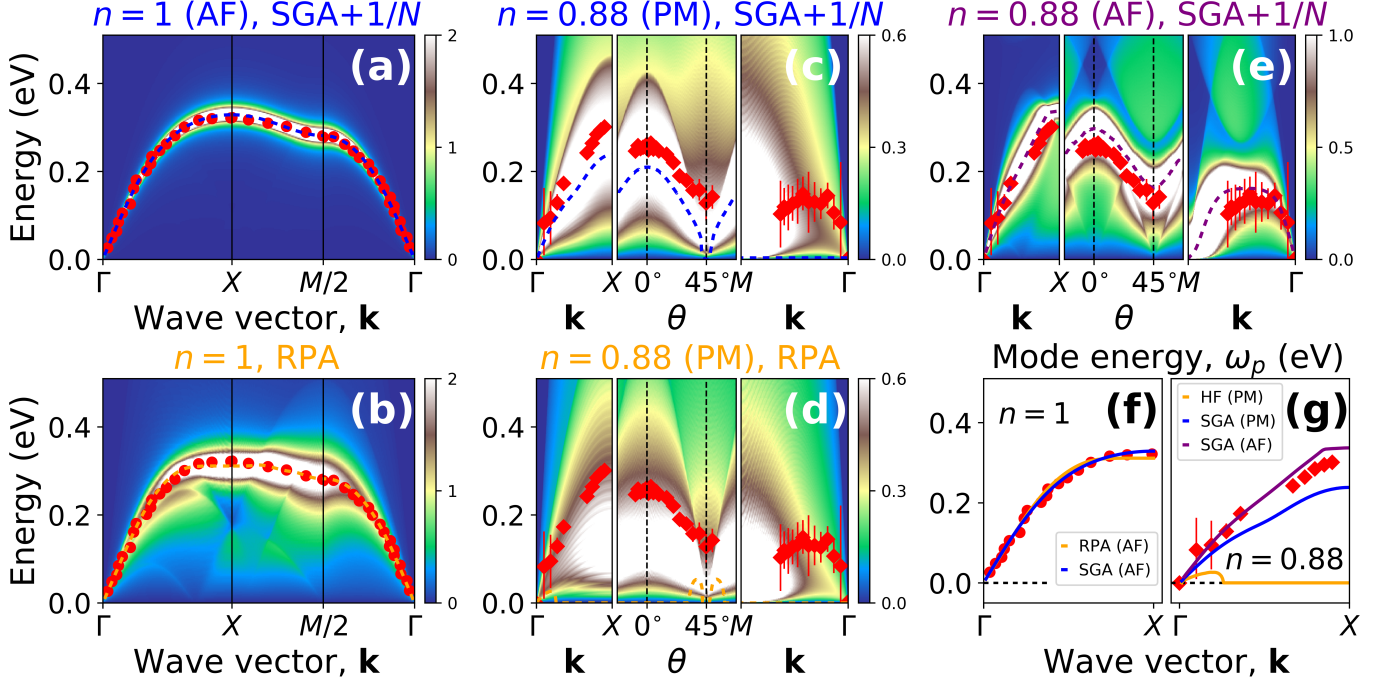


FIG. 1. Calculated quantum spin-fluctuation spectra for undoped AF insulator [$n = 1$; panels (a-b)], paramagnetic metal [$n = 0.88$; panels (c-d)], and antiferromagnetic metal [$n = 0.88$; panel (e)]. The model parameters are provided in Table I. Dashed lines in (a-e) represent real parts of the quasiparticle pole ω_p (the so-called propagation frequency), obtained by damped-harmonic-oscillator modeling of the numerical data as detailed in [41]. Experimental energies for La_2CuO_4 [INS; actually shifted by $\mathbf{q}_{\text{AF}} = (0.5, 0.5)$] and $\text{La}_{1.88}\text{Sr}_{0.12}\text{CuO}_4$ (RIXS) are taken from [42] and [26], respectively. Panels (f) and (g) provide the direct comparison of the calculated and experimental dispersions for $n = 1.0$ and $n = 0.88$, respectively. Angle θ in panels (c-e) parameterizes the Brillouin-zone arc $\mathbf{k}(\theta) \equiv 0.37 \cdot (\cos \theta, \sin \theta)$.

$-i[\bar{\eta}_{i+\delta i}^\alpha \eta_i^\beta - \bar{\eta}_i^\beta \eta_{i+\delta i}^\alpha]/2$, and corresponding composite fields $P_i^{(\alpha, \beta, \delta i, \text{Re/Im})} \propto \langle \hat{P}_i^{(\alpha, \beta, \delta i, \text{Re/Im})} \rangle$ accommodating collective modes. Here i and α are lattice- and joint spin-orbital indices, respectively. We consider the imaginary-time action

$$\mathcal{S} = \sum_i \int d\tau \eta_i^\dagger (\partial_\tau - \mu) \eta_i + \int d\tau E_G(\mathbf{P}_i, \{x\}) + i \sum_{ij} d\tau \xi_i^T (\hat{\mathbf{P}}_i - \mathbf{P}_i), \quad (1)$$

where the vector notation indicates internal index summations and $E_G \equiv \langle \Psi_G | \hat{\mathcal{H}} | \Psi_G \rangle / \langle \Psi_G | \Psi_G \rangle$ is the SGA energy, evaluated using Gutzwiller-type wave function $|\Psi_G(\{x\})\rangle$ [10, 11, 40] ($\{x\}$ is the set of correlator parameters). By application of Wick's theorem, E_G becomes a functional of \mathbf{P}_i and $\{x\}$. The last term in Eq. (1) is the constraint enforcing that the composite fields follow the Hamiltonian dynamics. Finally, E_G is expanded in fields \mathbf{P}_i up to quartic terms, and relevant correlation functions are evaluated to the leading non-trivial $1/N$ expansion order using the action \mathcal{S} . Susceptibility matrix is obtained by Fourier-transforming the expressions

$\hat{\chi}_{ij}(\tau, \tau') = \int \mathbf{P}_i(\tau) \mathbf{P}_j^T(\tau') \exp(-\mathcal{S})$, analytic continuation to real frequencies and unfolding them to the PM Brillouin zone. The current scheme is free of Fierz ambiguity, making standard $1/N$ phase diagrams strongly-dependent on unphysical parameters [43, 44]. This feature of the SGA+ $1/N$ constitutes an essential improvement as it allows for an unbiased comparison with experiment.

The model parameters adopted for $\text{La}_{2-x}\text{Sr}_x\text{CuO}_4$ (LSCO) and $(\text{Bi, Pb})_2(\text{Sr, La})_2\text{CuO}_{6+\delta}$ (Bi2201) are summarized in Table I. Temperature T is set so as to stay clear of spin-spiral states present in both HF and Gutzwiller phase diagrams [45]. This step allows to study PM state in the doping range inaccessible within previous $T = 0$ operator Gutzwiller-method extensions [46, 47]. Contrary to SGA+ $1/N$, application of RPA to the present situation requires violating hierarchy $k_B T \ll |t| \ll U$ (or, alternatively, taking unphysically small $U \approx 1.5|t|$ [23]), making it inadequate for the cuprates. Nevertheless, we present the RPA results for comparison. Numerical and phase-stability aspects are detailed in [41].

Results.—In Fig. 1 we display the calculated imaginary parts of transverse dynamical spin susceptibility along representative Brillouin-zone contours for

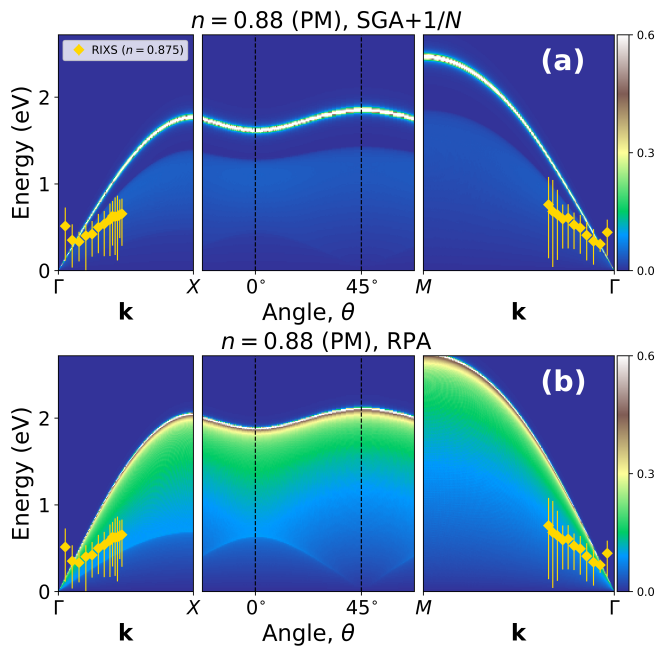


FIG. 2. Calculated imaginary part of the dynamical charge susceptibility, $|t|\chi_C''(\mathbf{k}, \omega)$, along selected Brillouin-zone contours for LSCO at $n = 0.88$ (cf. Table I for parameters). Panel (a) shows discrete charge-excitation mode splitting of the electron-hole continuum as obtained from SGA+1/N approach. Analogous results obtained from RPA (b) are displayed for comparison. In the latter situation the mode appears at the upper threshold of the continuum. Angle θ parameterizes the arc $\mathbf{k}(\theta) \equiv 0.37 \cdot (\cos \theta, \sin \theta)$. Diamonds are RIXS data for $\text{La}_{2-x}(\text{Br}, \text{Sr})_x\text{CuO}_4$ at $n = 0.875$ [15].

$\text{La}_{2-x}\text{Sr}_x\text{CuO}_4$ (see Table I for model parameters). Red symbols are the inelastic neutron scattering [42] and RIXS data for $\text{La}_{2-x}\text{Sr}_x\text{CuO}_4$ [26], respectively. In panels (a-b) we display the spin-wave spectrum for half-filled ($n = 1$) AF insulator, calculated using the present SGA+1/N (a) and RPA (b) techniques, both of which accurately reproduce the experimental data. This is no longer the case for the doped PM metal state ($n = 0.88$), as follows from Fig. 1(c-d), where only SGA+1/N results reproduce the trends in a semiquantitative manner. For reference, in Fig. 1(e), we display also SGA+1/N results for the commensurate AF state at slightly lower temperature (cf. Table I). The dashed lines in (a-e) are physical real parts of the quasiparticle pole, ω_p , extracted from the computed susceptibilities using the damped-harmonic-oscillator model [41]. The latter is controlled by bare frequency, ω_0 , and damping, γ ($\omega_p \equiv \sqrt{\omega_0^2 - \gamma^2}$ for $\omega_0 > \gamma$, otherwise $\omega_p = 0$ and the paramagnon is *overdamped*). Experimental points represent the same propagation frequency, ω_p . Note that, within RPA, paramagnons are overdamped already for $n = 0.88$ along all directions, whereas SGA+1/N result provides propagating ($\omega_p > 0$), but damped spin excitations along Γ -X direction and the contour following magnetic-zone boundary (cf. the

TABLE I. Summary of model parameters taken to fit the data for $\text{La}_{2-x}\text{Sr}_x\text{CuO}_4$ (LSCO) and $(\text{Bi}, \text{Pb})_2(\text{Sr}, \text{La})_2\text{CuO}_{6+\delta}$ (Bi2201). In each case, the next-nearest neighbor hopping is set to $t' = 0.25|t|$. Phases are marked as: AF – antiferromagnetic, and PM – paramagnetic; n is electron concentration.

System	Method	n	Phase	$ t $ (eV)	U (eV)	$k_B T$ (eV)
LSCO	SGA+1/N	1.0	AF	0.34	2.38	0.1224
LSCO	SGA+1/N	0.88	PM	0.34	2.38	0.1224
LSCO	SGA+1/N	0.88	AF	0.34	2.38	0.1122
LSCO	RPA	1.0	AF	0.34	2.38	0.4420
LSCO	RPA	0.88	PM	0.34	2.38	0.5168
Bi2201	SGA+1/N	0.97	AF	0.31	1.86	0.1116
Bi2201	SGA+1/N	< 0.97	PM	0.31	1.86	0.1116

middle panels), in agreement with experiment. The latter results constitute the crucial difference with those of RPA, cf. the explicit comparison of calculated energies ω_p with experimental data along the Γ -X line, provided in Fig. 1(f-g). The PM SGA+1/N calculation slightly overestimates damping along the nodal line [cf. right panel in (c)]. Experimentally, however, paramagnons at $n = 0.88$ are close to the overdamping along Γ -M direction and definitely lose propagating-mode characteristics at $n = 0.84$ [30]. Full quantitative agreement with RIXS is obtained for the doped AF SGA+1/N case (e). Such a residual magnetic order might be indeed present, since the measurements have been performed at the verge of the stripe phase [48]. In brief, magnetism turns out not to be the crucial factor for the overall spectrum shape, except for the Γ -M line, where it extends the stability region of magnetic modes. We emphasize that the same Hamiltonian parameters were used in SGA+1/N calculations, both for the undoped ($n = 1$) and doped ($n = 0.88$) systems (cf. Table I). No direct doping-dependence of either the hopping or the Coulomb parameters is necessary to reproduce the data in those two cases. Parenthetically, this may also suggest that $d_{x^2-y^2}$ - d_{z^2} hybridization is less relevant to magnetic excitations than previously concluded in terms of the effective Heisenberg-model description [26].

For the sake of completeness, the impact of the local correlations on the charge dynamics is illustrated in Fig. 2. The color intensity represents imaginary part of the dynamical charge susceptibility $|t|\chi_C''(\mathbf{k}, \omega)$ for LSCO at $n = 0.88$ (cf. Table I), obtained within both SGA+1/N (a) and RPA (b) approximations. Only SGA+1/N yields a clear discrete mode that separates from the continuum. Such a splitting has been also noted within t - J - V models [49]. Since the charge mode in the cuprates has three-dimensional character [16] and is sensitive to long-range Coulomb interactions (not included in the Hubbard model), this part of analysis is only qualitative. For reference, we show the measured charge mode energies for $\text{La}_{2-x}(\text{Br}, \text{Sr})_x\text{CuO}_4$ at $n = 0.875$ (diamonds) [15].

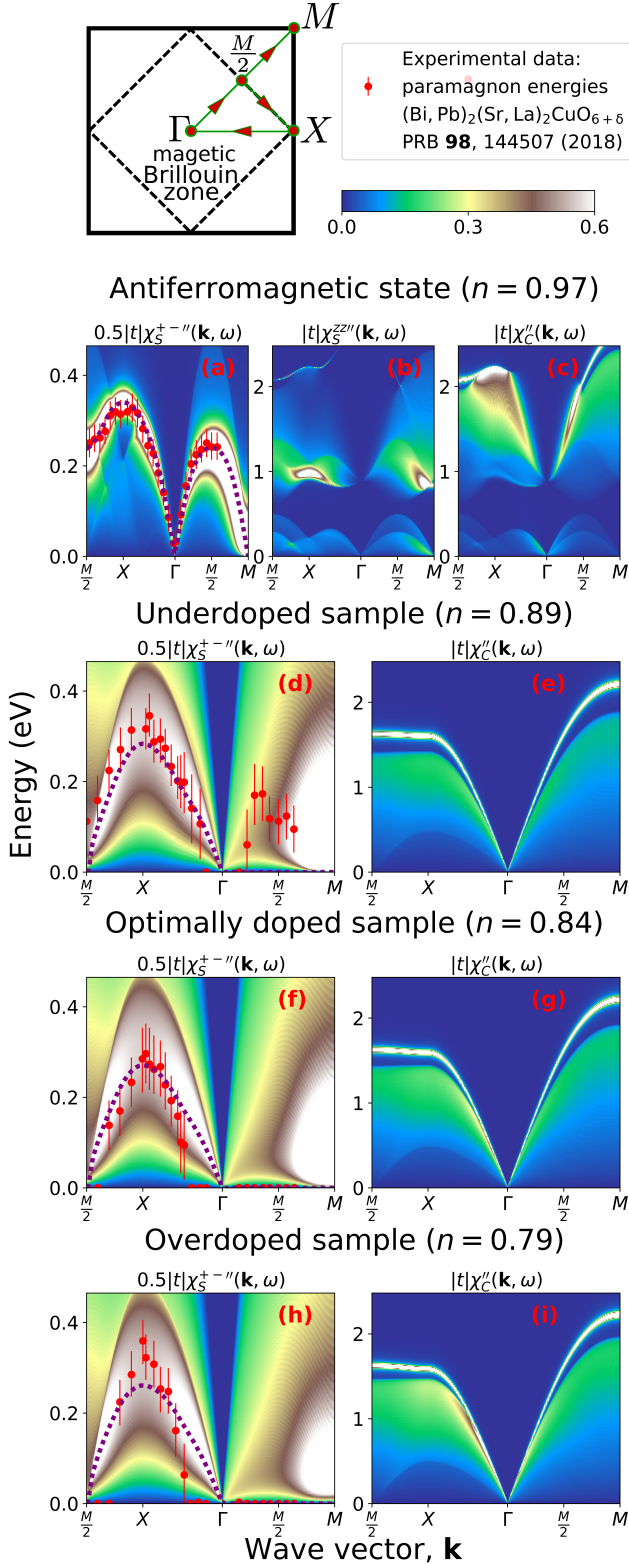


FIG. 3. Spin- and charge-dynamic susceptibilities, χ_S^{+-} , χ_S^{zz} , and χ_C calculated using the present SGA+1/ N approach. Red circles correspond to RIXS data for (Bi, Pb)₂(Sr, La)₂CuO_{6+δ} [33]. Note different energy scales for the spin- and charge modes. For computational details see [41]. The Brillouin zone contour for panels (a-i) is shown at the top.

To demonstrate a universal character of the relationship between local correlations and paramagnons, we provide in Fig. 3 the same SGA+1/ N analysis for the second cuprate family, (Bi, Pb)₂(Sr, La)₂CuO_{6+δ} (Bi2201). In the present situation smaller U and $|t|$ were taken to match the excitation energies in the AF state (cf. Table I). Panels (a-d) exhibit calculated dynamical spin susceptibilities for AF state ($n = 0.97$) and PM phase ($n = 0.89, 0.84, 0.79$). Dashed lines represent theoretical values of the propagation frequencies and red circles are the RIXS data [33]. The agreement is quantitative along the $\frac{M}{2}$ - X - Γ contour at all doping levels, from AF insulator ($n = 0.97$) to overdoped PM metal ($n = 0.79$), except for narrow regions where the paramagnon energies, a strong damping is seen in both experimental and calculations for doped samples, and is marked by the dotted $\omega = \omega_p = 0$ line in Fig. 3(d-f). PM SGA+1/ N solution yields paramagnon overdamping for n larger by no more than 0.05 from that observed experimentally. The imaginary part of the longitudinal spin susceptibility ($\chi_S^{zz''}$) in the AF state is plotted Fig. 3(b). A clear separation of the low-energy and high-energy parts of the e-h continuum is seen in $\chi_S^{zz''}$. Close to the M -point, the amplitude mode emerges from the e-h continuum. For the PM case, the corresponding longitudinal part is not displayed as it is equivalent to the transverse susceptibility by the symmetry. Finally, panels (c-i) express calculated imaginary part of the dynamical charge susceptibility. The main qualitative effect of the electronic correlations is detachment of the sharp charge mode from the e-h continuum. This is a non-perturbative effect that does not occur in weak-coupling calculation (cf. Fig. 2).

Discussion.—In correlated electron systems close to localization, Mott physics and magnetic dynamics are well separated and governed by the Hubbard U and kinetic exchange interaction $J \sim 4t^2/U$, respectively. The combined SGA+1/ N and RPA study (cf. Figs. 1 and 3) points towards mutual intertwining of these two scales, manifesting itself by persistence of paramagnons in hole-doped systems. The low-energy ϕ^4 -type effective models (renormalized by integrating out high-energy fermion dynamics), despite their success for normal metals, may thus be not appropriate starting point to study collective modes in HTSC materials. The relationship between charge-, spin-, and superconducting fluctuations may be qualitatively understood by invoking the identity $\hat{\mathbf{S}}_i \hat{\mathbf{S}}_j - \frac{1}{4} \hat{n}_i \hat{n}_j \equiv -\hat{B}_{ij}^\dagger \hat{B}_{ij}$ [50], where $\hat{B}_{ij}^\dagger \equiv \frac{1}{\sqrt{2}} (\hat{c}_{i\uparrow}^\dagger \hat{c}_{j\downarrow}^\dagger - \hat{c}_{i\downarrow}^\dagger \hat{c}_{j\uparrow}^\dagger)$ is the spin-singlet creation operator, whereas $\hat{\mathbf{S}}_i$ and \hat{n}_i are local-spin and particle-number operators, respectively. This interdependence is augmented by the correlation-driven renormalization of hopping which can easily become of the order of J and thus those two processes coexist and balance out each other in the relevant doping range. The saddle-

point (SGA [40]) solution and its DE-GWF extension (including short-range correlations [10]) provide stable AF [51], charge-density-wave [52] or HTSC [10] phases, whereas the long-range fluctuations around those states, expressed by the action (1), are well accounted for by the extension presented here. In our view, the previous quantitative study of equilibrium and single-particle properties of HTSC [10, 11, 52], combined with the systematic generalization to the collective-quantum-excitation description, provides an argument for a decisive role of strong correlations in high- T_c cuprates. These results can be tested further by generalizing such a picture to the t - J - U or three-band HTSC models.

Acknowledgment.—This work was supported by Grant OPUS No. UMO-2018/29/B/ST3/02646 from Narodowe Centrum Nauki (NCN).

* maciej.fidrysiak@uj.edu.pl

† jozef.spalek@uj.edu.pl

- [1] S. Hüfner, M. A. Hossain, A. Damascelli, and G. A. Sawatzky, “Two gaps make a high-temperature superconductor?” *Rep. Prog. Phys.* **71**, 062501 (2008).
- [2] T. Yoshida, M. Hashimoto, I. M. Vishik, Z.-X. Shen, and A. Fujimori, “Pseudogap, Superconducting Gap, and Fermi Arc in High- T_c Cuprates Revealed by Angle-Resolved Photoemission Spectroscopy,” *J. Phys. Soc. Japan* **81**, 011006 (2012).
- [3] B. Keimer, S. A. Kivelson, M. R. Norman, S. Uchida, and J. Zaanen, “From quantum matter to high-temperature superconductivity in copper oxides,” *Nature* **518**, 179 (2015).
- [4] C. Proust and L. Taillefer, “The Remarkable Underlying Ground States of Cuprate Superconductors,” *Annual Review of Condensed Matter Physics* **10**, 409 (2019).
- [5] M. Ogata and H. Fukuyama, “The t - J model for the oxide high- T_c superconductors,” *Rep. Prog. Phys.* **71**, 036501 (2008).
- [6] M. Randeria, R. Sensarma, and N. Trivedi, *Projected Wavefunctions and High T_c Superconductivity in Doped Mott Insulators* (Springer Berlin Heidelberg, 2011) pp. 29–64.
- [7] J. Kaczmarczyk, J. Bünemann, and J. Spalek, “High-temperature superconductivity in the two-dimensional t - J model: Gutzwiller wavefunction solution,” *New J. Phys.* **16**, 073018 (2014).
- [8] H. Alloul, “What is the simplest model that captures the basic experimental facts of the physics of underdoped cuprates?” *Compt. Rend. Physique* **15**, 519 (2014).
- [9] N. E. Hussey, J. Buhot, and S. Licciardello, “A tale of two metals: contrasting criticalities in the pnictides and hole-doped cuprates,” *Rep. Prog. Phys.* **81**, 052501 (2018).
- [10] J. Spalek, M. Zegrodnik, and J. Kaczmarczyk, “Universal properties of high-temperature superconductors from real-space pairing: t - J - U model and its quantitative comparison with experiment,” *Phys. Rev. B* **95**, 024506 (2017).
- [11] M. Fidrysiak, M. Zegrodnik, and J. Spalek, “Realistic estimates of superconducting properties for the cuprates: reciprocal-space diagrammatic expansion combined with variational approach,” *J. Phys.: Condens. Matter* **30**, 475602 (2018).
- [12] L. J. P. Ament, G. Ghiringhelli, M. M. Sala, L. Braicovich, and J. van den Brink, “Theoretical Demonstration of How the Dispersion of Magnetic Excitations in Cuprate Compounds can be Determined Using Resonant Inelastic X-Ray Scattering,” *Phys. Rev. Lett.* **103** (2009).
- [13] M. W. Haverkort, “Theory of Resonant Inelastic X-Ray Scattering by Collective Magnetic Excitations,” *Phys. Rev. Lett.* **105** (2010).
- [14] L. Braicovich, J. van den Brink, V. Bisogni, M. Moretti Sala, L. J. P. Ament, N. B. Brookes, G. M. De Luca, M. Salluzzo, T. Schmitt, V. N. Strocov, and G. Ghiringhelli, “Magnetic Excitations and Phase Separation in the Underdoped $\text{La}_{2-x}\text{Sr}_x\text{CuO}_4$ Superconductor Measured by Resonant Inelastic X-Ray Scattering,” *Phys. Rev. Lett.* **104**, 077002 (2010).
- [15] K. Ishii, T. Tohyama, S. Asano, K. Sato, M. Fujita, S. Wakimoto, K. Tustsui, S. Sota, J. Miyawaki, H. Niwa, and et al., “Observation of momentum-dependent charge excitations in hole-doped cuprates using resonant inelastic x -ray scattering at the oxygen K edge,” *Phys. Rev. B* **96**, 115148 (2017).
- [16] M. Hepting, L. Chaix, E. W. Huang, R. Fumagalli, Y. Y. Peng, B. Moritz, K. Kummer, N. B. Brookes, W. C. Lee, M. Hashimoto, and et al., “Three-dimensional collective charge excitations in electron-doped copper oxide superconductors,” *Nature* **563**, 374 (2018).
- [17] K. Ishii, M. Kurooka, Y. Shimizu, M. Fujita, K. Yamada, and J. Mizuki, “Charge Excitations in $\text{Nd}_{2-x}\text{Ce}_x\text{CuO}_4$ Observed with Resonant Inelastic X-ray Scattering: Comparison of Cu K -edge with Cu L_3 -edge,” *J. Phys. Soc. Japan* **88**, 075001 (2019).
- [18] R. Fumagalli, L. Braicovich, M. Minola, Y. Y. Peng, K. Kummer, D. Betto, M. Rossi, E. Lefrançois, C. Morawe, M. Salluzzo, and et al., “Polarization-resolved Cu L_3 -edge resonant inelastic x -ray scattering of orbital and spin excitations in $\text{NdBa}_2\text{Cu}_3\text{O}_{7-\delta}$,” *Phys. Rev. B* **99**, 134517 (2019).
- [19] J. Q. Lin, Jie Yuan, Kui Jin, Z. P. Yin, Gang Li, Ke-Jin Zhou, Xingye Lu, M. Dantz, Thorsten Schmitt, H. Ding, Haizhong Guo, M. P. M. Dean, and X. Liu, “Doping evolution of the charge excitations and electron correlations in electron-doped superconducting $\text{La}_{2-x}\text{Ce}_x\text{CuO}_4$,” (2019), arXiv:1906.11354.
- [20] M. P. M. Dean, G. Dellea, R. S. Springell, F. Yakhov-Harris, K. Kummer, N. B. Brookes, X. Liu, Y.-J. Sun, J. Strle, T. Schmitt, and et al., “Persistence of magnetic excitations in $\text{La}_{2-x}\text{Sr}_x\text{CuO}_4$ from the undoped insulator to the heavily overdoped non-superconducting metal,” *Nat. Mater.* **12**, 1019 (2013).
- [21] K. Ishii, M. Fujita, T. Sasaki, M. Minola, G. Dellea, C. Mazzoli, K. Kummer, G. Ghiringhelli, L. Braicovich, T. Tohyama, and et al., “High-energy spin and charge excitations in electron-doped copper oxide superconductors,” *Nat. Commun.* **5**, 3714 (2014).
- [22] W. S. Lee, J. J. Lee, E. A. Nowadnick, S. Gerber, W. Tabiś, S. W. Huang, V. N. Strocov, E. M. Motoyama, G. Yu, B. Moritz, and et al., “Asymmetry of collective excitations in electron- and hole-doped cuprate superconductors,” *Nat. Phys.* **10**, 883 (2014).

- [23] M. Guarise, B. Dalla Piazza, H. Berger, E. Giannini, T. Schmitt, H. M. Rønnow, G. A. Sawatzky, J. van den Brink, D. Altenfeld, I. Eremin, and et al., “Anisotropic softening of magnetic excitations along the nodal direction in superconducting cuprates,” *Nat. Commun.* **5**, 5760 (2014).
- [24] S. Wakimoto, K. Ishii, H. Kimura, M. Fujita, G. Dellea, K. Kummer, L. Braicovich, G. Ghiringhelli, L. M. Debeer-Schmitt, and G. E. Granroth, “High-energy magnetic excitations in overdoped $\text{La}_{2-x}\text{Sr}_x\text{CuO}_4$ studied by neutron and resonant inelastic x -ray scattering,” *Phys. Rev. B* **91** (2015).
- [25] M. Minola, Y. Lu, Y. Y. Peng, G. Dellea, H. Gretarsson, M. W. Haverkort, Y. Ding, X. Sun, X. J. Zhou, D. C. Peets, and et al., “Crossover from Collective to Incoherent Spin Excitations in Superconducting Cuprates Probed by Detuned Resonant Inelastic X-Ray Scattering,” *Phys. Rev. Lett.* **119**, 245133 (2017).
- [26] O. Ivashko, N. E. Shaik, X. Lu, C. G. Fatuzzo, M. Dantz, P. G. Freeman, D. E. McNally, D. Destraz, N. B. Christensen, T. Kurosawa, and et al., “Damped spin excitations in a doped cuprate superconductor with orbital hybridization,” *Phys. Rev. B* **95** (2017).
- [27] Y. Y. Peng, G. Dellea, M. Minola, M. Conni, A. Amorese, D. Di Castro, G. M. De Luca, K. Kummer, M. Salluzzo, X. Sun, and et al., “Influence of apical oxygen on the extent of in-plane exchange interaction in cuprate superconductors,” *Nat. Phys.* **13**, 1201 (2017).
- [28] D. Meyers, H. Miao, A. C. Walters, V. Bisogni, R. S. Springell, M. d’Astuto, M. Dantz, J. Pelliciani, H. Y. Huang, J. Okamoto, and et al., “Doping dependence of the magnetic excitations in $\text{La}_{2-x}\text{Sr}_x\text{CuO}_4$,” *Phys. Rev. B* **95**, 075139 (2017).
- [29] L. Chaix, E. W. Huang, S. Gerber, X. Lu, C. Jia, Y. Huang, D. E. McNally, Y. Wang, F. H. Vernay, A. Keren, and et al., “Resonant inelastic x -ray scattering studies of magnons band bimagnons in the lightly doped cuprate $\text{La}_{2-x}\text{Sr}_x\text{CuO}_4$,” *Phys. Rev. B* **97**, 155144 (2018).
- [30] H. C. Robarts, M. Barthelemy, M. Garcia-Fernandez, J. Li, A. Nag, A. C. Walters, K. J. Zhou, and S. M. Hayden, “Anisotropic damping of the spin fluctuations in doped $\text{La}_{2-x}\text{Sr}_x\text{CuO}_4$ studied by resonant inelastic x -ray scattering,” (2019), arXiv:1908.03086.
- [31] M. Le Tacon, G. Ghiringhelli, J. Chaloupka, M. Moretti Sala, V. Hinkov, M. W. Haverkort, M. Minola, M. Bakr, K. J. Zhou, S. Blanco-Canosa, and et al., “Intense paramagnon excitations in a large family of high-temperature superconductors,” *Nat. Phys.* **7**, 725 (2011).
- [32] C. J. Jia, E. A. Nowadnick, K. Wohlfeld, Y. F. Kung, C.-C. Chen, S. Johnston, T. Tohyama, B. Moritz, and T. P. Devereaux, “Persistent spin excitations in doped antiferromagnets revealed by resonant inelastic light scattering,” *Nat. Commun.* **5** (2014).
- [33] Y. Y. Peng, E. W. Huang, R. Fumagalli, M. Minola, Y. Wang, X. Sun, Y. Ding, K. Kummer, X. J. Zhou, N. B. Brookes, and et al., “Dispersion, damping, and intensity of spin excitations in the monolayer $(\text{Bi, Pb})_2(\text{Sr, La})_2\text{CuO}_{6+\delta}$ cuprate superconductor family,” *Phys. Rev. B* **98** (2018).
- [34] K.-J. Zhou, Y.-B. Huang, C. Monney, X. Dai, V. N. Strocov, N.-L. Wang, Z.-G. Chen, C. Zhang, P. Dai, L. Patthey, and et al., “Persistent high-energy spin excitations in iron-pnictide superconductors,” *Nat. Commun.* **4**, 1470 (2013).
- [35] H. Gretarsson, N. H. Sung, J. Porras, J. Bertinshaw, C. Dietl, Jan A. N. Bruin, A. F. Bangura, Y. K. Kim, R. Dinnebier, Jungho Kim, and et al., “Persistent Paramagnons Deep in the Metallic Phase of $\text{Sr}_{2-x}\text{La}_x\text{IrO}_4$,” *Phys. Rev. Lett.* **117**, 107001 (2016).
- [36] D. J. Scalapino, “A common thread: The pairing interaction for unconventional superconductors,” *Rev. Mod. Phys.* **84**, 1383 (2012).
- [37] A. V. Chubukov, D. Pines, and J. Schmalian (Springer Berlin Heidelberg, 2003) Chap. A Spin Fluctuation Model for d -Wave Superconductivity, pp. 495–590.
- [38] P. W. Anderson, “Is There Glue in Cuprate Superconductors?” *Science* **316**, 1705 (2007).
- [39] P. A. Lee, N. Nagaosa, and X.-G. Wen, “Doping a Mott insulator: Physics of high-temperature superconductivity,” *Rev. of Mod. Phys.* **78**, 17 (2006).
- [40] J. Jędrak and J. Spałek, “Renormalized mean-field t - J model of high- T_c superconductivity: Comparison to experiment,” *Phys. Rev. B* **83**, 104512 (2011).
- [41] M. Fidrysiak and J. Spałek, “Supplemental Material,”.
- [42] N. S. Headings, S. M. Hayden, R. Coldea, and T. G. Perring, “Anomalous High-Energy Spin Excitations in the High- T_c Superconductor-Parent Antiferromagnet La_2CuO_4 ,” *Phys. Rev. Lett.* **105** (2010).
- [43] J. Jaeckel and C. Wetterich, “Flow equations without mean field ambiguity,” *Phys. Rev. D* **68**, 025020 (2003).
- [44] T. Baier, E. Bick, and C. Wetterich, “Temperature dependence of antiferromagnetic order in the Hubbard model,” *Phys. Rev. B* **70**, 125111 (2004).
- [45] P. A. Igoshev, M. A. Timirgazin, V. F. Gilmudinov, A. K. Arzhnikov, and V. Yu Irkhin, “Spiral magnetism in the single-band Hubbard model: the Hartree-Fock and slave-boson approaches,” *J. Phys.: Condens. Matter* **27**, 446002 (2015).
- [46] G. Seibold and J. Lorenzana, “Time-Dependent Gutzwiller Approximation for the Hubbard Model,” *Phys. Rev. Lett.* **86**, 2605 (2001).
- [47] G. Seibold and J. Lorenzana, “Doping dependence of spin excitations in the stripe phase of high- T_c superconductors,” *Phys. Rev. B* **73**, 144515 (2006).
- [48] K. Yamada, C. H. Lee, K. Kurahashi, J. Wada, S. Wakimoto, S. Ueki, H. Kimura, Y. Endoh, S. Hosoya, G. Shirane, and et al., “Doping dependence of the spatially modulated dynamical spin correlations and the superconducting-transition temperature in $\text{La}_{2-x}\text{Sr}_x\text{CuO}_4$,” *Phys. Rev. B* **57**, 6165 (1998).
- [49] A. Greco, H. Yamase, and M. Bejas, “Plasmon excitations in layered high- T_c cuprates,” *Phys. Rev. B* **94**, 075139 (2016).
- [50] J. Spałek, “Effect of pair hopping and magnitude of intratomic interaction on exchange-mediated superconductivity,” *Phys. Rev. B* **37**, 533 (1988).
- [51] M. Abram, M. Zegrodnik, and J. Spałek, “Antiferromagnetism, charge density wave, and d -wave superconductivity in the extended t - J - U model: role of intense Coulomb interaction and a critical overview of renormalized mean field theory,” *J. Phys.: Condens. Matter* **29**, 365602 (2017).
- [52] M. Zegrodnik and J. Spałek, “Incorporation of charge- and pair-density-wave states into the one-band model of d -wave superconductivity,” *Phys. Rev. B* **98**, 155144 (2018).
- [53] J. Kaczmarczyk, J. Spałek, T. Schickling, and J. Büne-

- mann, “Superconductivity in the two-dimensional Hubbard model: Gutzwiller wave function solution,” *Phys. Rev. B* **88**, 115127 (2013).
- [54] J. A. M. Vermaseren, “New features of FORM,” (2000), arXiv:math-ph/0010025 [math-ph].

Supplemental Material

STATISTICALLY-CONSISTENT-GUTZWILLER (SGA) + 1/N METHOD

Here we provide some of the details of the SGA+1/N technique that we have developed to study magnetic and charge fluctuations in correlated lattice systems.

The general Hamiltonian that we consider is of the t - J - U - V form

$$\hat{\mathcal{H}} = \sum_{ij\alpha\beta\sigma} t_{ij}^{\alpha\beta} \hat{c}_{i\sigma}^{\alpha\dagger} \hat{c}_{j\sigma}^{\beta} + \sum_{i\alpha} U^{\alpha} \hat{n}_{i\uparrow}^{\alpha} \hat{n}_{i\downarrow}^{\alpha} + \sum'_{ij\alpha\beta} J_{ij}^{\alpha\beta} \hat{\mathbf{S}}_i^{\alpha} \hat{\mathbf{S}}_j^{\beta} + \sum_{ij\alpha\beta} V_{ij}^{\alpha\beta} \hat{n}_i^{\alpha} \hat{n}_j^{\beta}, \quad (\text{S1})$$

where i, j and α, β denote lattice and orbital indices, respectively. Primes indicate summations over unique pairs of distinct indices. The consecutive terms denote hopping, Hubbard- U , intersite Coulomb repulsion, and exchange interactions. Note that, even though here we restrict ourselves to the single-band case, the orbital index is necessary due to the cell-doubling in the antiferromagnetic state.

The starting point is the statistically-consistent approach [7, 10, 40, 53] which is based on the variational energy functional $E_G \equiv \langle \Psi_G | \mathcal{H} | \Psi_G \rangle / \langle \Psi_G | \Psi_G \rangle$ with the variational state $|\Psi_G\rangle \equiv \hat{P}_G |\Psi_0\rangle$. Here $|\Psi_0\rangle$ is ‘‘uncorrelated’’ wave function (Slater determinant), $\hat{P}_G \equiv \prod_{i\alpha} \hat{P}_{G_i}^{\alpha}$ with

$$\hat{P}_{G_i}^{\alpha} \equiv (\lambda_{i0}^{\alpha} |0\rangle_{ii} \langle 0| + \lambda_{i\uparrow\downarrow}^{\alpha} |\uparrow\rangle_{ii} \langle \downarrow| + \lambda_{i\downarrow\uparrow}^{\alpha} |\downarrow\rangle_{ii} \langle \uparrow| + \lambda_{i\uparrow\uparrow}^{\alpha} |\uparrow\rangle_{ii} \langle \uparrow| + \lambda_{i\downarrow\downarrow}^{\alpha} |\downarrow\rangle_{ii} \langle \downarrow| + \lambda_{id}^{\alpha} |\uparrow\downarrow\rangle_{ii} \langle \uparrow\downarrow|) \quad (\text{S2})$$

is the correlator (controlled locally by six λ -parameters) that adjusts local many-body configurations in the variational wave function in response to interactions, and $P_{\gamma} \equiv \langle \Psi_0 | \hat{P}_{\gamma} | \Psi_0 \rangle$ are uncorrelated expectation values of the bilinears $\hat{P}_{\gamma} \equiv \hat{c}_{i\sigma}^{\alpha\dagger} \hat{c}_{j\sigma'}^{\alpha'}$, where $\gamma = (ij\alpha\alpha'\sigma\sigma')$ is the joint spin-lattice-orbital index. We require that \hat{P}_G is Hermitian which implies that λ_{i0}^{α} , $\lambda_{i\sigma\sigma}^{\alpha}$, and λ_{id}^{α} are real, whereas $\lambda_{i\uparrow\downarrow}^{\alpha} = \lambda_{i\downarrow\uparrow}^{\alpha*}$. In the absence of spin-orbit coupling, the off-diagonal terms may be safely set to zero as long as the variational ground-state is considered. However, here we will discuss fluctuations that, in general, induce a non-zero values of $\lambda_{i\uparrow\downarrow}^{\alpha}$ and $\lambda_{i\downarrow\uparrow}^{\alpha}$.

The statistically-consistent-Gutzwiller free energy functional reads

$$\mathcal{F}_{\text{SGA}} = -\frac{1}{\beta} \ln \text{Tr} \exp \left[-\beta E_G(\mathbf{P}, \boldsymbol{\lambda}) + \beta \boldsymbol{\xi}^{\dagger} (\mathbf{P} - \hat{\mathbf{P}}) + \beta \mu (\hat{N}_e - N_e) \right], \quad (\text{S3})$$

where we have used bold-symbol vector-notation to write down internal-index summations in a compact manner and $\beta \equiv 1/k_B T$ is the inverse temperature. This expression is next optimized with respect to bilinear expectation values \mathbf{P} and correlator parameters λ_{α} under the constraint of fixed particle number. Additionally, a constraint $\mathbf{P} = \langle \hat{\mathbf{P}} \rangle$ is enforced by additional set of Lagrange multipliers $\boldsymbol{\xi}$. This step assures that the variational expectation values coincide with those evaluated using the Bogoliubov-de Gennes self-consistent equations. Finally, five more constraints are added for the correlator parameters, $\langle (\hat{P}_{G_i}^{\alpha})^2 \hat{c}_{i\sigma}^{\alpha\dagger} \hat{c}_{i\sigma'}^{\alpha} \rangle_0 \equiv \langle \hat{c}_{i\sigma}^{\alpha\dagger} \hat{c}_{i\sigma'}^{\alpha} \rangle_0$, and $\langle (\hat{P}_{G_i}^{\alpha})^2 \rangle_0 \equiv 1$. Note that this method, contrary to the usual variational energy optimization, is applicable also at non-zero temperature. This is essential in the present context as it allows to stay clear of spin-spiral states ubiquitous for Hubbard-type models, both at Hartree-Fock and the saddle-point solution levels at low temperature [45].

The functional (S3) is of saddle-point type and does not capture the long-wavelength collective modes. We now incorporate them by starting from an improved functional

$$\mathcal{F}_{\text{SGA}+1/N} = -\frac{1}{\beta} \ln \int \mathcal{D}[\bar{\boldsymbol{\eta}}, \boldsymbol{\eta}] \mathcal{D}\mathbf{P}_i \mathcal{D}\boldsymbol{\xi}_i \exp(-\mathcal{S}), \quad (\text{S4})$$

with the action

$$\mathcal{S} = \int_i d\tau \boldsymbol{\eta}_i(\tau)^{\dagger} (\partial_{\tau} - \mu) \boldsymbol{\eta}_i(\tau) + \int d\tau E_G(\mathbf{P}_i(\tau), \{x\}) + i \int_{ij} d\tau \boldsymbol{\xi}_i(\tau)^{\dagger} (\hat{\mathbf{P}}_i(\tau) - \mathbf{P}_i(\tau)), \quad (\text{S5})$$

where $\boldsymbol{\eta}_i(\tau)$ are Grassman fields and the meaning of remaining symbols in Eq. (S5) remains the same as in Eq. (S3), except for non-trivial imaginary-time dependence. At this point, it is also understood that all the constraints for the correlator parameters have been already solved, so that $\lambda_{i\beta}^{\alpha} = \lambda_{i\beta}^{\alpha}(x_i^{\alpha})$ with a single variational parameter, x_i^{α} (there are five constraints for six coefficients per orbital).

Note that the saddle point solution of (S4) coincides *exactly* with that obtained from the SGA functional (S3). The SGA+1/N extension [cf. Eq. (S4)] allows, however, to compute fluctuation corrections to both static and dynamic quantities. Technically, this is done by expanding the energy functional $E_G(\mathbf{P}_i(\tau), \{x\})$ in the time-dependent composite fields $\mathbf{P}_i(\tau)$ to quartic order and evaluating the resulting free energy $\mathcal{F}_{\text{SGA}+1/N}$ using 1/N expansion technique, with N being the number of fermionic flavors. Finally, dynamical spin- and charge susceptibility matrices are evaluated to the leading non-trivial order in 1/N, starting from the SGA solution.

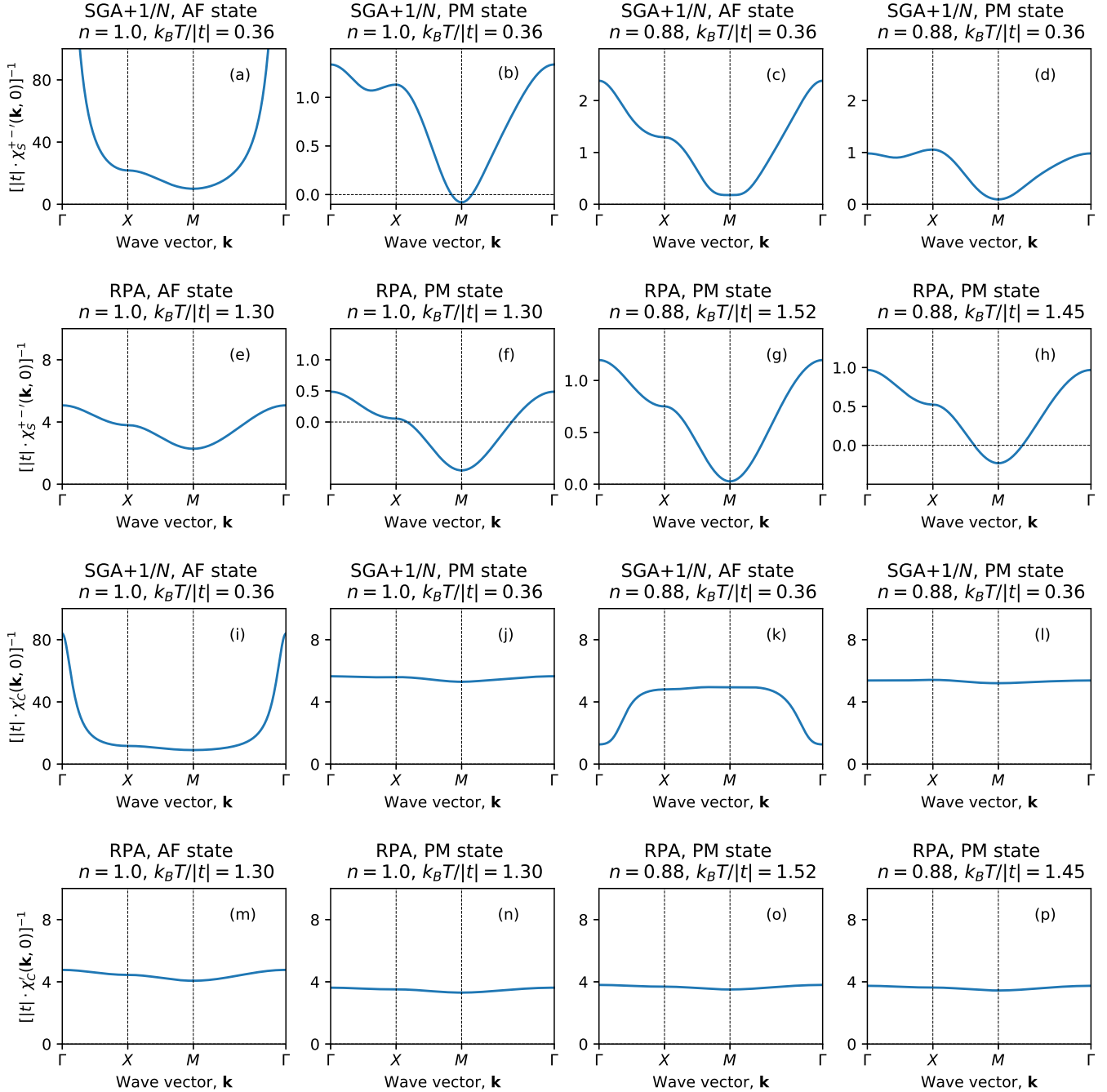


FIG. S1. Inverse of the real part of the static ($\omega = 0$) longitudinal spin- [panels (a-h)] and charge- [panels (i-p)] susceptibility for antiferromagnetic (AF) and paramagnetic (PM) states as a function of wave vector. The model parameters are: $t = -0.34$, $t' = 0.25|t|$, $U = 7|t|$. Calculations were performed using the present SGA+1/ N method [panels (a-d) and (i-l)] and RPA [panels (e-h) and (m-p)]. Temperature and doping level are displayed on the top of each panel.

NUMERICAL DETAILS

In this analysis we restrict to the Hubbard model with next- and next-nearest-neighbor hopping, $t < 0$ and $t' = 0.25|t|$, respectively. Aside from tests and benchmarks (encompassing symmetry analysis in external applied Zeeman field and for various microscopic Hamilto-

nians), the exchange and intersite Coulomb interactions have been set to zero. The model parameters for two considered cuprate compounds, $\text{La}_{2-x}\text{Sr}_x\text{CuO}_4$ (electron concentration $n = 1, 0.88$) and $(\text{Bi, Pb})_2(\text{Sr, La})_2\text{CuO}_{6+\delta}$ ($n = 0.97, 0.89, 0.84, 0.79$) are summarized in Table I of the main text. All calculations have been performed at $T > 0$ for $N \times N$ two-site magnetic cells ($N = 300$;

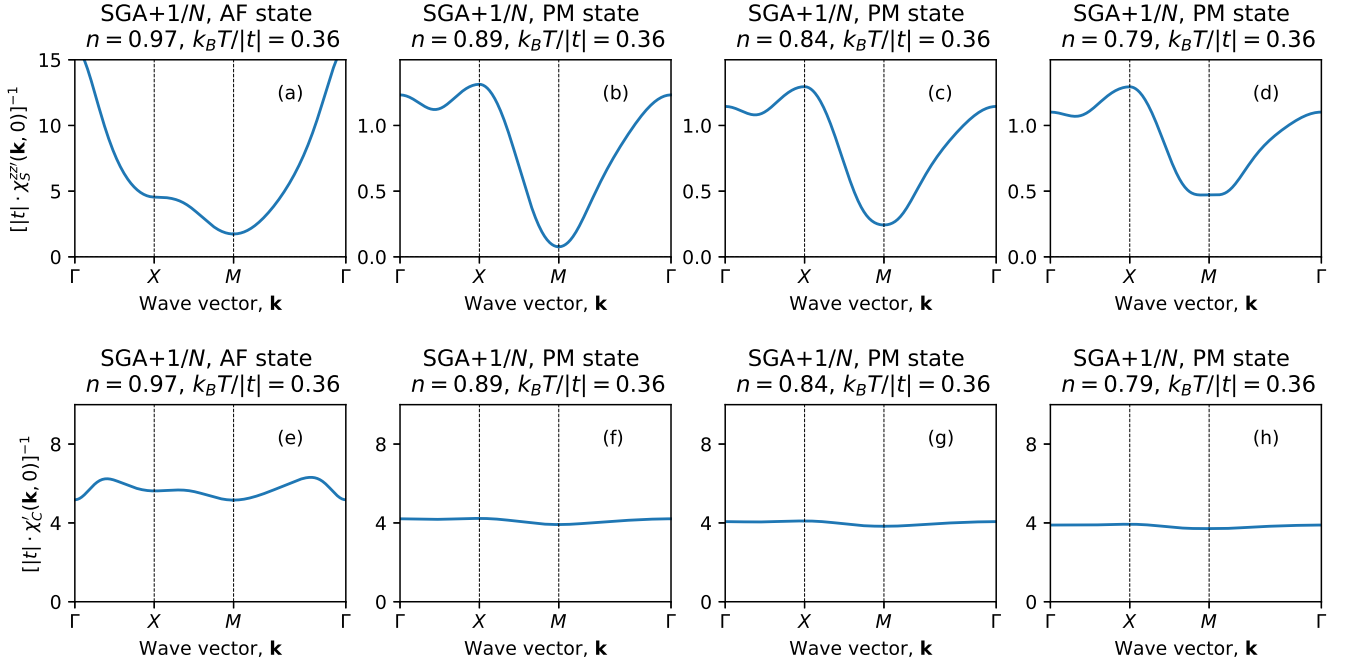


FIG. S2. Inverse of the real part of static ($\omega = 0$) longitudinal spin- [panels (a-h)] and charge- [panels (i-p)] susceptibility for antiferromagnetic (AF) and paramagnetic (PM) states as a function of wave vector, calculated using the present SGA+1/N method at various doping levels. The model parameters are: $t = -0.31$ eV, $t' = 0.25|t|$, $U = 6|t|$. Temperature is set to $k_B T = 0.36|t|$ for all the dopings specified.

18×10^4 sites in total) with imposed periodic boundary conditions. A mesh of 200 frequencies was used to generate the dynamical susceptibility color maps of and a small imaginary part was added to frequency while performing analytic continuation $i\omega_n \rightarrow \omega + i\epsilon$ with $\epsilon = 0.008|t|$. While computing real parts of susceptibility ϵ was set to zero, but small uniform \mathbf{k} -space disorder was introduced to minimize finite-size effects. The target absolute accuracy for dimensionless variational parameters was set to 10^{-10} . Algorithmic Hamiltonian block-reduction was implemented at the level of variational calculation and susceptibility-matrix evaluation. Monte Carlo tree-search algorithm (MCTS) implemented in FORM system [54] was used for symbolic energy functional optimization. GNU Scientific Library was employed for multidimensional optimization and matrix operations. The computations were performed on a dedicated supercomputer EDABI (Jagiellonian University, Kraków, Poland).

PHASE STABILITY

A successful optimization of the variational free-energy functional does not ensure the solution stability in the presence of higher-order effects, such as fluctuation corrections. Here we demonstrate that, for the selection of temperatures provided in Table I of the main text, all the considered phases are stable against spin

and charge fluctuations. In Fig. S1(a-h) we plot inverse real part of the zero-frequency dynamical longitudinal spin susceptibility for the parameters employed for $\text{La}_{2-x}\text{Sr}_x\text{CuO}_4$ ($t = -0.34$, $t' = 0.25|t|$, $U/|t| = 7$). The undoped system ($n = 1$) exhibits stable commensurate AF state within the SGA+1/N approximation for $k_B T = 0.36|t| \ll |t|$ [cf. (a)], whereas paramagnetic state is unstable against magnetic fluctuations (b). For the same temperature, SGA+1/N yields stable PM state for doped ($n = 0.88$) system [panel (c)] and commensurate AF state for slightly lowered $k_B T = 0.33|t|$ (d). To obtain a similar behavior within RPA approximation, one needs to break the hierarchy of energies $k_B T \ll |t| \ll U$, as demonstrated in panels (e-h). In particular, even for $k_B T = 1.45|t| > |t|$ the system is magnetically unstable at $n = 0.88$ (h), which renders RPA inadequate in the strong-coupling regime. Similar analysis for charge susceptibilities, summarized in panels (i-p), shows that there are no dynamical instabilities to charge ordered phases for the selected parameter values.

We have also performed a similar analysis for the parameters suitable for $(\text{Bi, Pb})_2(\text{Sr, La})_2\text{CuO}_{6+\delta}$ (Bi2201). The results are summarized in Fig. S2, proving the dynamical stability of the SGA+1/N solution against spin and charge fluctuations for all considered doping levels.

Finally, it is instructive to observe how the extensively studied [45] incommensurate phases emerge as the temperature is lowered. For $n = 0.88$, starting from the

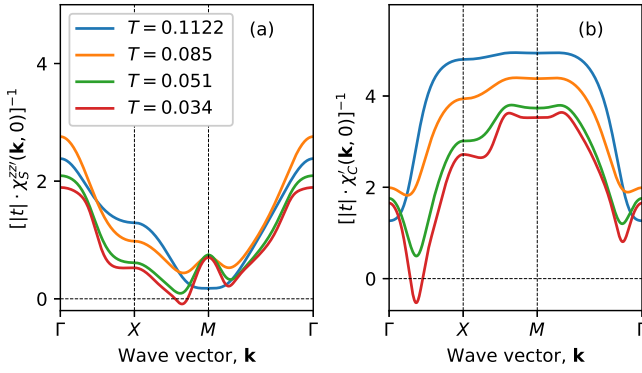


FIG. S3. Inverse of the real part of static ($\omega = 0$) longitudinal spin (a) and charge (b) susceptibility for AF state and $n = 0.88$, calculated using the present SGA+1/N approach. The model parameters are $t = -0.34$ eV, $t' = 0.25|t|$, $U = 7|t|$. Temperatures in panel (a) are given in eV. As temperature is lowered, a near simultaneous dynamical incommensurate spin- and charge-instability of the AF state is generated.

PM phase, a commensurate AF state appears around $k_B T = 0.33|t|$. A further cooling generates near instantaneous spin- and charge- dynamical instability of the AF order, as demonstrated in Fig. S3. By proper selection of temperature, one can thus stay clear of incommensurate magnetic states.

DAMPED HARMONIC OSCILLATOR MODELING OF THE SGA+1/N AND RPA RESULTS: DETAILS OF FITTING THE DATA

Whereas the principal result of the present contribution is evaluation of the magnetic response functions for strongly-correlated states (cf. color maps Figs. 1 and 3 of main text), comparison of obtained theoretical results with available experimental data requires further processing. In this section, we describe this secondary analysis.

The experimental RIXS spectra are typically modeled by the dissipative part of damped harmonic-oscillator response of the form

$$\chi''_{\text{oscillator}}(\mathbf{k}, \omega) = \frac{2F(\mathbf{k})\gamma(\mathbf{k})\omega}{[\omega^2 - \omega_0^2(\mathbf{k})]^2 + 4\gamma(\mathbf{k})^2\omega^2}, \quad (\text{S6})$$

with the particle-hole and multi-magnon background added extra. Here $\omega_0(\mathbf{k})$ and $\gamma(\mathbf{k})$ are wave-vector-dependent bare frequency and damping coefficients, and $F(\mathbf{k})$ is scaling factor. Equation (S6) describes a *damped propagating* mode (paramagnon) of energy $\omega_p(\mathbf{k}) \equiv \sqrt{\omega_0^2(\mathbf{k}) - \gamma^2(\mathbf{k})}$ if $\omega_0 > \gamma$. Otherwise, for $\gamma > \omega_0$, the quasiparticle pole becomes purely imaginary and the mode is *overdamped*. Apart from ω_0 and ω_p , one can

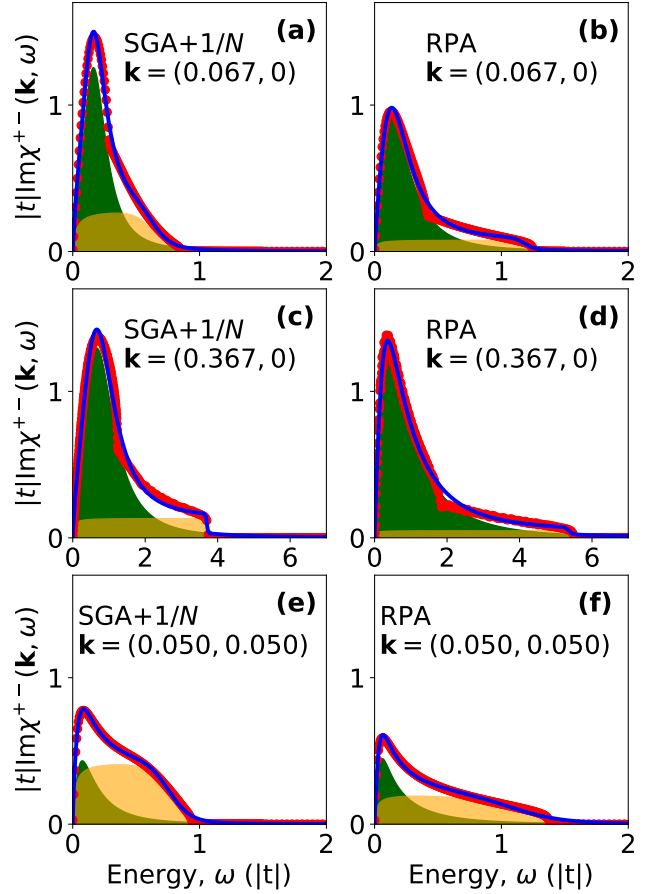


FIG. S4. Exemplary fits of the total dissipative part of susceptibility $\chi''_{\text{total}} \equiv \chi''_{\text{oscillator}} + \chi''_{\text{incoh}}$ (blue solid curve) to the imaginary part of dynamical susceptibility $\text{Im}\chi^{+-}(\mathbf{k}, \omega)$ calculated using SGA+1/N [panels (a), (c), (e)] and RPA [panels (b), (d), (f)] (red circles) for doping $n = 0.88$. The wave vectors, \mathbf{k} , in the panels are given in the units of $2\pi/a$ with a being lattice spacing. The damped-oscillator and background partial contributions are marked in green and orange, respectively.

also define the third frequency, ω_{max} , for which expression (S6) attains maximum. Physically, the most relevant one, and also reported in many of the experimental works, is ω_p that we also provide in the present study.

We introduce particle-hole background of the form

$$\chi''_{\text{incoh}} \equiv \frac{A(\mathbf{k})\omega}{1 + B(\mathbf{k})\omega} n_F[C(\mathbf{k})(\omega - D(\mathbf{k}))], \quad (\text{S7})$$

where $n_F(x) \equiv (\exp(x) + 1)^{-1}$ is the Fermi function, and A, B, C, D are positive \mathbf{k} -dependent coefficients. This function describes a featureless continuum that is softly cut off on the low-energy side and suppressed above threshold $\omega \sim D$. We have found that the function (S7) is flexible enough to accurately model the particle-hole background in the wide doping range. Note that none

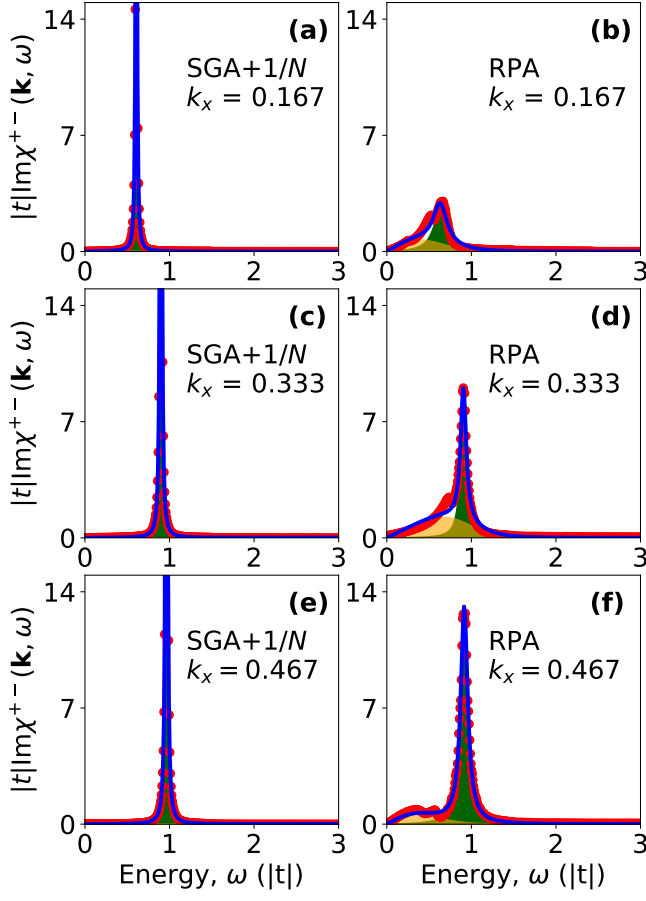


FIG. S5. Same as in Fig. S4, but at half-filling ($n = 1$). The sharp peaks represent a true magnon excitation in the stable AF phase.

of the employed approximations accounts for the weak multi-magnon peak, seen in some RIXS experiments [30]. Hence, there is no need to subtract this feature.

In Fig. S4 we show exemplary fits of the total dissipative part of susceptibility $\chi''_{\text{total}} \equiv \chi''_{\text{oscillator}} + \chi''_{\text{incoh}}$ (blue solid curve) to the imaginary part of dynamical susceptibility $\chi^{+-}(\mathbf{k}, \omega)$, calculated using the present SGA+1/N (left panels) and RPA (right panels) approximations. The total response is decomposed into a step-like particle-hole continuum (orange color) and the peak that is modeled by a damped harmonic oscillator (displayed in green). From Fig. S4(a-f) it is apparent that *the main effect of electronic correlations is to compress the incoherent part of the spectrum and reduce the paramagnon damping* (these correlations are incorporated only into the SGA+1/N calculation). However, the magnetic peak maximum ω_{max} is actually shifted to higher energies due to local Hubbard-interaction physics [as seen particularly well in panels (c) and (d)]. This effect is counterintuitive as it opposes the behavior of the incoherent excitations that are transferred to lower energy,

but it is necessary to match the experimental data for the cuprates. Similar fits, performed at half-filling ($n = 1$) are shown in Fig. S5. In this case the sharp coherent peak is a true magnon excitation and a small residual background represents residual particle-hole excitations, present for $T > 0$ and in the situation with not too strong correlations ($U/|t| \sim 7$).